Available online at www.sciencedirect.com
ScienceDirect
Surface & Coatings Technology 202 (2008) 2113–2120
SURFACE & COATINGS TECHNOLOGY
www.elsevier.com/locate/surfcoat

Microstructure of reaction zone in WC_p/duplex stainless steels matrix composites processing by laser melt injection

A.M. Do Nascimento [a], V. Ocelík [b,*], M.C.F. Ierardi [a], J.Th.M. De Hosson [b]

[a] *Department of Materials Science, Faculty of Mechanical Engineering, State University of Campinas, UNICAMP, P.O. Box 6122, 13083-970 Campinas — SP, Brazil*
[b] *Department of Applied Physics, Zernike Institute for Advanced Materials and Netherlands Institute for Metals Research, University of Groningen, Nijenborgh 4, 9747 AG Groningen, The Netherlands*

Received 13 June 2007; accepted in revised form 28 August 2007
Available online 7 September 2007

Abstract

The laser melt injection (LMI) process has been used to create a metal matrix composite consisting of 80μm sized multi-grain WC particles embedded in three cast duplex stainless steels. The microstruture was investigated by scanning electron microscopy with integrated EDS and electron back-scatter diffraction/orientation imaging microscopy. In particular the search of the processing parameters, e.g. laser power density, laser beam scanning speed and powder flow rate, to obtain crack free and WC_p containing surface layer, has been examined. Before the injection of ceramic particles into remelted surface layer, the influence of processing parameters of laser surface remelting on the microstructure and properties of selected duplex steels was also investigated. Although after simple laser surface remelting the austenitic phase is almost not present inside remelted layer, in the case of LMI the austenite was observed in vicinity of WC particles, due to increase of carbon content acting as austenite stabilizer. The diffusion of carbon in the reaction zone results also in a formation of W_2C phase in the neighborhood of WC particles with a strong orientation relationship between them. The maximum volume fraction of the particles achieved in the metal matrix composite layer was about 10% and a substantial increase in hardness was observed, i.e. 575 HV0.2 for the matrix with embedded particles in comparison to 290 HV0.2 for untreated cast duplex stainless steels.

Keywords: Laser treatment; Metal matrix composite; Electron back-scatter diffraction; Duplex stainless steel

1. Introduction

The injection of ceramic particles into a melt pool, which is created in the top of a metal substrate by a high power laser beam [1–4] may form metal matrix-ceramic composite (MMC) layers on metal surfaces. The main goal of this laser melt injection (LMI) process is to improve mechanical and chemical properties of metal surfaces such as steels, Al or Ti alloys. Surface layers prepared by the LMI process exhibit strong bonding and no large discontinuity of properties at the layer/substrate interface [5].

The overall properties of the MMC layer depend on the specific properties and amount of injected ceramic particles, on the microstructure of the laser beam remelted substrates and on the presence and properties of new phases formed by chemical reactions between matrix and particles. These phases are mainly present at the particle/matrix interface in the so-called reaction zone.

Cast duplex stainless steel (CDSS) have been used in many industrial processes for special purposes in the chemical, petrochemical, fertilizer and cellulose industries [6–8]. They are generally used as compressor cylinders, digester valves, feed screws, impellers, liners, pump casings, runway light fixtures (aircraft carriers, airports), safety valves, sprocket wheels, pistons, seal rings (centrifugal pumps) and valve parts due to excellent corrosion resistance. However, their mechanical properties, mainly hardness and wear resistance, may be insufficient in some applications and therefore decreasing the life time of the component [9]. In the literature there are several

* Corresponding author. Tel.: +31 50 363 3407; fax: +31 50 363 4881.
E-mail address: v.ocelik@rug.nl (V. Ocelík).

0257-8972/$ - see front matter © 2007 Elsevier B.V. All rights reserved.
doi:10.1016/j.surfcoat.2007.08.065

Table 1
The chemical composition (in wt.%) of the three types of CDSSs: ASTM A890 grade 1A (free of nitrogen), ASTM A890 grade 3A (with nitrogen and without Cu) and ASTM A890 grade 6A (Super Duplex)

Alloy	C	Cr	Ni	Mn	Si	Mo	S	P	Cu	N	W	Cr/Ni	PRE
1A	0.04	25.01	5.53	0.78	0.99	2.11	0.006	0.026	3.10			3.52	31.97
3A	0.03	25.33	5.38	0.84	0.90	2.13	0.005	0.025		0.19		2.70	35.96
6A	0.02	25.96	7.93	0.83	0.97	3.63	0.008	0.024	0.82	0.24	0.78	2.17	43.07

All compositions are balanced to 100% by iron. In last two columns the ratio of Cr and Ni equivalents, and pitting resistant equivalent are shown, respectively. Cr_{eq}=%Cr+%Mo+0.7x%Nb [18]; Ni_{eq}=%Ni+35x%C+20x%N+0.25x%Cu [18]; PRE=%Cr+3.3(%Mo+0.5%W)+16%N [33].

attempts to improve the surface properties of different steels via formation of coatings by laser surface modification techniques mainly by laser cladding and alloying, using WC particles mixed with Co or Ni alloys as clad powders [10–17].

This work is aimed at examining the microstructural changes in the three types of CDSSs representing different groups of these materials after laser surface remelting and LMI of WC particles. The final objective of the project is to improve the mechanical properties and the wear resistance of different duplex steels.

2. Experimental details

Laser experiments have been carried out with a continuous wave 2kW Rofin Sinar Nd-YAG laser. The detailed sketch for laser melt injection set-up can be found elsewhere [3,5]. The laser beam is used to create melt pool at the surface of moving metallic substrate and simultaneously ceramic particles are injected into the melt pool just behind the laser beam using glass nozzle and Argon as carrier gas. The laser beam is positioned at an 11° angle with respect to the substrate surface normal to avoid harmful reflections from the specimen back into the optical fiber. Argon was used as a shielding gas to protect the lens as well as to reduce oxidation of the specimen. The spot size of the laser beam on the work piece was 2.8mm with an approximately Gaussian distribution of laser beam power. Four axes CNC table was employed for specimen movement.

The CDSSs used in our experiments with their chemical compositions, Cr_{eq}/Ni_{eq} ratios and estimated pitting resistance equivalents [18,33] are shown in Table 1. Circular plates with dimensions ϕ50mm × 10mm were used as a substrate material. Before laser treatment, the surface has been sandblasted to promote the absorption of the laser light. A powder feeding system Sulzer Metco Twin 10C supplied WC multi-grain particles with an average size of about 80μm, using Ar as a carrier gas with flow rate of 67ml/s. The particles were injected into the melt pool at an angle of 37° with respect to the surface normal.

Standard light microscopy (Olympus Vanox-AHTM), scanning electron microscopy (SEM Philips XL30 FEG), Orientation Imaging Microscopy (TSL attachment to Philips XL30 FEG) and XRD diffraction (Philips PW-1830, CuKα radiation)

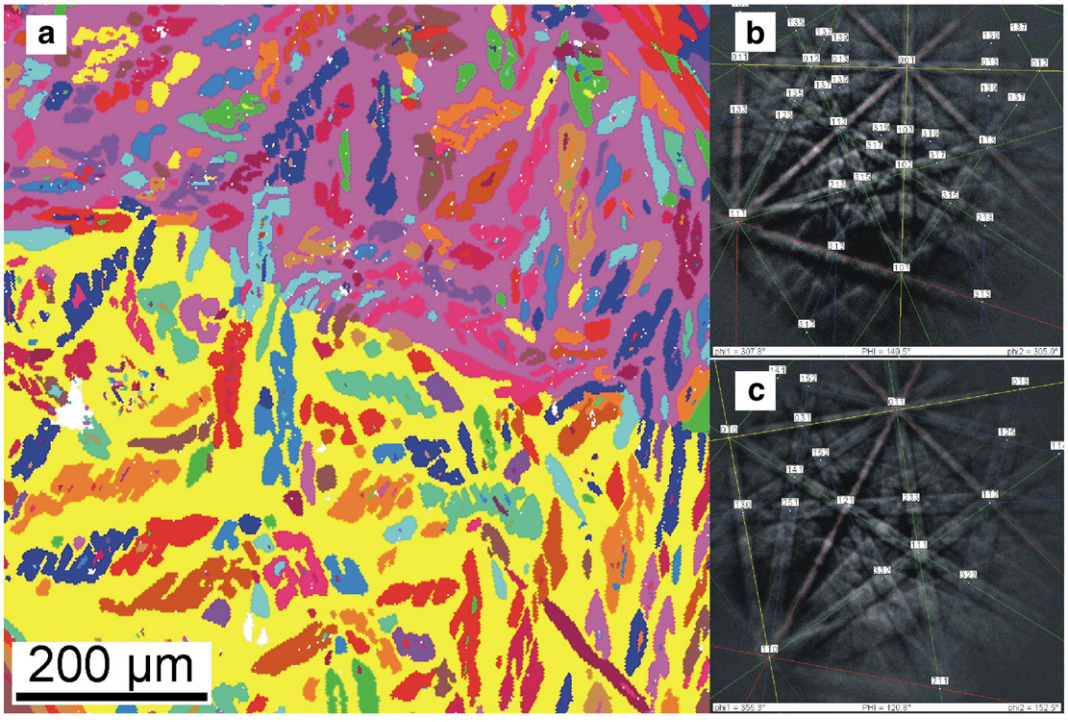

Fig. 1. The microstructure of 6A duplex steel studied by orientation imaging microscopy in SEM. a) Austenitic dendrites distributed in two large ferritic grains. b) and c) are typical back-scattering electron diffraction patterns indexed as ferrite and austenite, respectively.

were used to study particle distribution, microstructure and microstructural orientation relationships (OR) in WC_p/CDSS layers prepared by injection of multi-grain WC particles into CDSS substrates.

Vickers hardness measurement is used to obtain information of the mechanical properties of transformed zone and substrate. The measurements were performed on cross-sections of the samples that have been ground and polished to eliminate the macro-roughness.

3. Results

During solidification the CDSS first solidifies as ferrite and when temperature decreases, austenite is developed [19]. The characteristic microstructure for CDSSs is the microstructure of austenitic islands in the ferritic matrix. Fig. 1a shows this typical microstructure for 6A alloy.

The grains of ferrite are coarse with a size ranging from 0.5 to 1mm and the mean size of austenite dendrites is about 30μm arranged in a few hundreds of micrometers long lines. As results of X-ray diffraction confirmed (see Fig. 4), austenite and ferrite are the main constituent phases for all three substrate alloys. The content of austenitic phase measured by OIM was almost the same (about 50%) for alloys 1A and 3A, but slightly lower (43%) for alloy 6A. A more detailed study of the orientation relationship between ferritic and austenitic grains in these three alloys showed that some differences in intensity of OR exist [20].

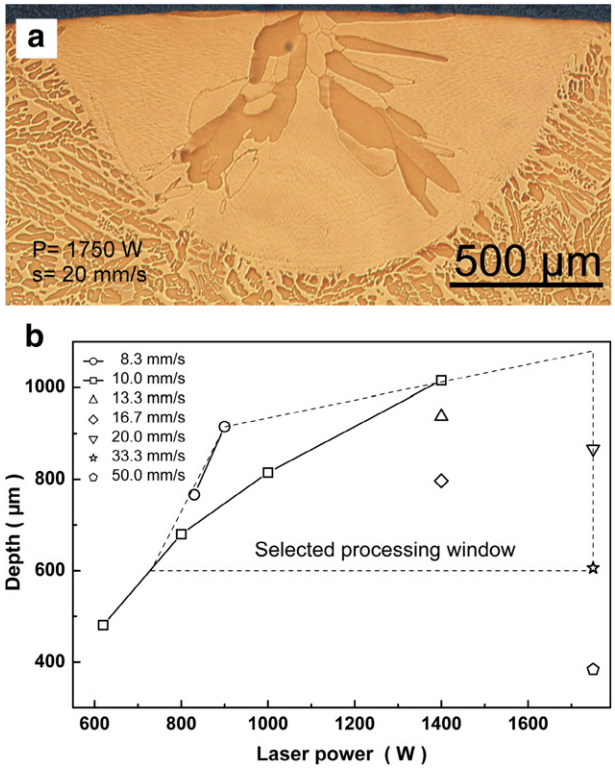

Fig. 2. a) Optical micrograph of characteristic shape of laser beam remelted surface area in a perpendicular cross-section made on 1A alloy at laser power 1750 W and scanning speed of 20 mm/s. b) Maximal depth of remelted single laser track as a function of laser power and laser beam scanning speed.

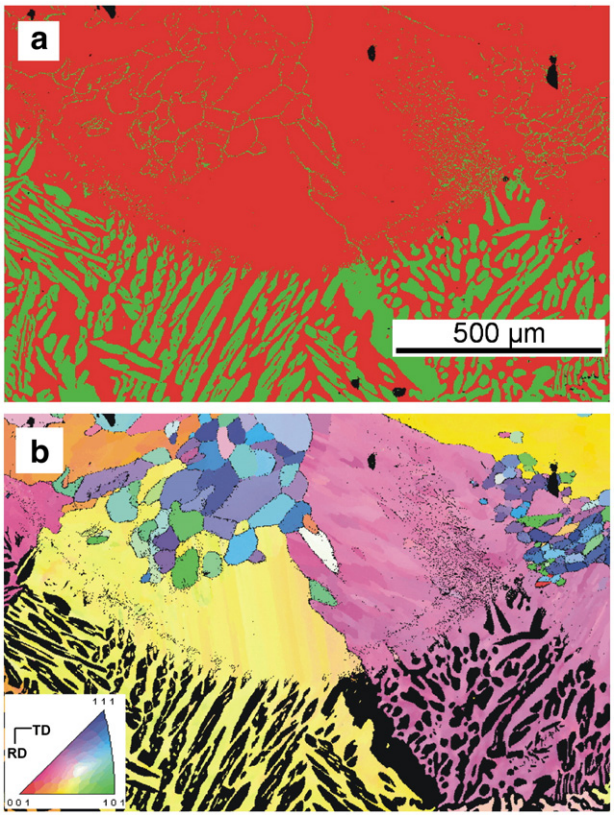

Fig. 3. OIM of remelted microstructure in the area of two overlapped laser tracks in 1A alloy. a) Phase mapping shows a predominant presence of ferrite (dark phase) in the remelted zone while in the substrate the both phases are almost equally present. b) Inverse pole figure from the same area shows the orientation of detected ferritic grains.

Fig. 2a shows a typical transversal cross-section of a single laser track produced by laser surface remelting. The aim of remelting experiments was to study the behavior of these alloys in the interaction with high power laser beam and to find a processing window of laser parameters for the further laser melt injection treatment. A characteristic shape of remelted zone for Gaussian type of beam energy distribution inside laser beam was observed. A substantial number of single remelting tracks were realized varying laser beam energy between 620 and 1750W and laser beam scanning speed between 8.33 and 50mm/s. The width of the remelted zone was close to the width of laser beam spot and did change only slightly with laser beam energy and scanning speed. The dependence of the maximal depth of remelted zone on laser beam power and scanning speed is summarized in Fig. 2b. As the final thickness of the transformed zone created by a partial overlapping of subsequent laser tracks should not be less than 300μm, we limited our processing window, as marked in Fig. 2b by the dashed line. It is important to note, that for all combinations of processing parameters the remelted single tracks were free of cracks or pores.

Fig. 3 shows the microstructure of the remelted surface and substrate in the area of overlapping of two laser tracks studied by OIM on transversal cross-section, using the overlap ratio of 33%. Fig. 3a highlights the present phases, whereas Fig. 3b shows

ferritic grains with different orientations. It is clear that after resolidification the microstructure is substantially changed. Fig. 3a demonstrates that the ferritic phase is dominant in remelted zone. Austenite nuclei are present at the grain boundaries of ferritic grains, but due to relatively high cooling rates during laser remelting, austenite is not further developed. Fig. 3b shows that the ferrite grains in remelted zone close to the interface with substrate follow the crystallographic orientation of grains from substrate but more close to the surface a new system of equiaxial ferritic grains with size between 50 and 200μm is formed.

The predominance of ferritic phase after laser remelting was confirmed by X-ray diffraction phase analysis for all three duplex steels. Fig. 4 presents XRD diffraction spectra of all three CDSSs for untreated and remelted state. It is possible to see that the austenite peaks decrease their relative intensities or disappear completely after laser remelting. The XRD spectra after remelting do not reveal any new peaks.

Fig. 5 shows the microhardness profiles of 3A alloy samples treated with different laser remelting parameters. An increase between 30 and 50% in hardness was observed in the remelted region for low and high scanning speeds, respectively. The increase of the hardness may be explained by microstructural changes, which are usually considered as important factor in driving the increase of hardness in the laser surface remelted alloys [21]. The laser beam scanning speed is one of the most important parameters because it mainly determines the solidification rate and the final microstructure. Between remelted zone and substrate material a heat affected zone is present with a thickness of about 200μm for all scanning speeds. The hardness inside this zone after a sharp change gradually decreases to the value of about 270 HV0.2, which is a typical value for non-treated material.

WC particles with a mean diameter of 80μm were injected in CDSSs round substrates (ϕ = 50mm) 10mm thick. Three subsequent laser tracks were created during rotation of the substrate under treated Nd:YAG laser beam using a synchronized lateral movement in such a way, that after one rotation the displacement between laser tracks of 1.5mm is achieved. We found that the processing window for successful laser melt injection is quite small. A special attention has been paid to set-up the regime, when particles have sufficient velocity to penetrate into the melt and they are not overheated or melted by the laser beam when they reach the melt substrate surface. This constraint requires an existence of melt pool 'tail' after the laser illuminated area [5] which shifts the processing windows towards higher scanning speeds and laser power densities. On the other side the higher laser power density can easily overheat or melt that part of injected particles which are even in a short contact with laser beam. These two rather opposite constraints squeeze the processing window for laser melt injection as it was

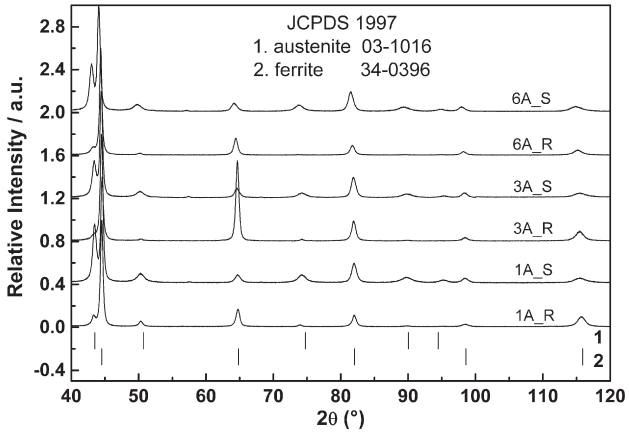

Fig. 4. Comparison of XRD spectra measured before (S) and after (R) laser surface remelting for all three CDSSs from Table 1. Positions of main XRD spectra lines for austenite and ferrite phase from JCPDS database are indicated.

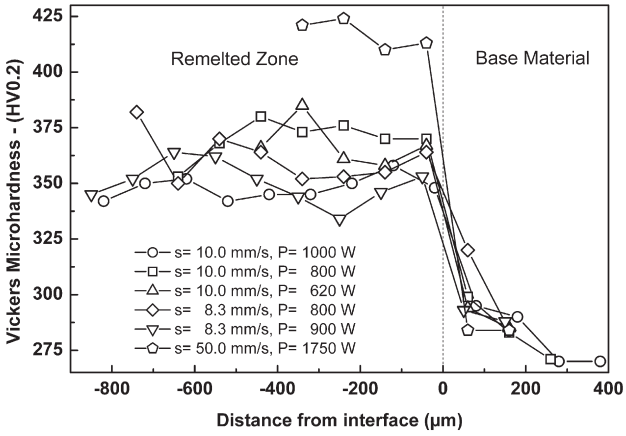

Fig. 5. Microhardness depth profiles measured on transversal cross-sections of laser tracks made with different processing parameters on 3A alloy. Each point shows the average value from three indents performed at the same depth. The first measurement starts at depth of 50 μm from the surface. Vertical line marks the position of boundary between the remelted and the substrate material.

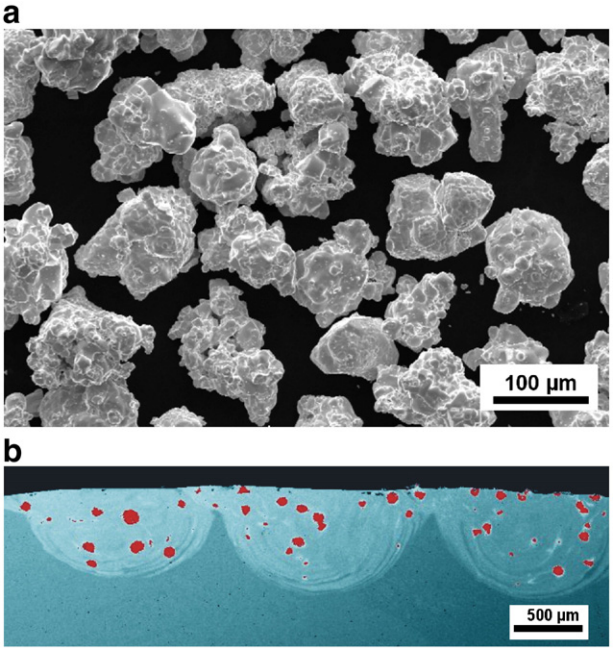

Fig. 6. a) SEM micrograph of WC particles. b) Light microscopy micrograph from perpendicular cross-section of three subsequent laser tracks with injected WC particles. Contrast for WC is enhanced via image manipulation software to estimate the volume fraction of injected particles.

observed earlier in case of Al, Ti and their alloys [1–5]. Due to the small size of processing window; it is quite difficult to manipulate the amount of injected particles, especially when a higher volume fraction of injected particles is required. An increase of powder feeding rate over some critical value always results in the substantial cracking of solidified laser track with cracks oriented mainly perpendicular to the cladding direction. Fig. 6a shows the shape and size of WC particles before injection and Fig. 6b is the optical micrograph of a transversal cross-section showing the distribution of injected particles in three partially overlapping laser tracks made with laser power of 1000W, laser beam scanning speed of 13.3mm/s and powder feeding rate of 73mg/s. This combination of processing parameters leads to the highest volume density of injected particles (8–10vol.%) without forming cracks inside the processed volume.

Fig. 7 shows the result of microhardness measurements performed on perpendicular cross-sections of LMI tracks to characterize hardness of the material between injected particles. After comparison with Fig. 5 it is clear that laser melt injection of WC particles increases the hardness more than simple laser surface remelting. The hardness is now almost doubled in comparison with non-treated substrates. This suggests that a substantial amount of W and C must be dissolved in the matrix. This was confirmed by EDS measurements, when an average value of 2.1at.% of W was measured in matrix areas between individual particles. One may conclude from it, that although during the LMI process a direct contact between injected particle and laser beam is minimized, some of the particles must be in a short contact with laser beam and therefore their surface has been melted. This melt was during injection mixed with the melt of substrate and formed a new matrix composition. Results in Fig. 7 also confirm that hardness value of the matrix after injection does not depend on duplex steel composition, while the initial hardness of 6a duplex steel substrate is a little bit higher than hardness for two others.

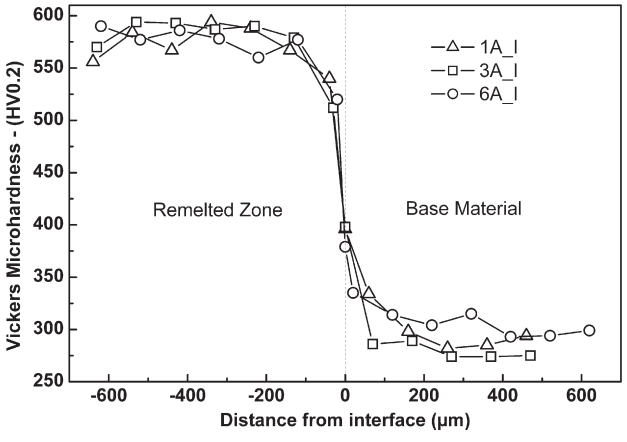

Fig. 7. Microhardness depth profiles measured on perpendicular cross-sections of laser tracks with injected WC particles for all three duplex steel alloys. During the measurements a direct indentation of WC particles was avoided to characterize only the hardness of matrix material between particles. Each point shows the average value from three indents performed at the same depth. The first measurement starts at depth of 50 μm from surface. Vertical line marks the position of boundary between remelted and substrate material.

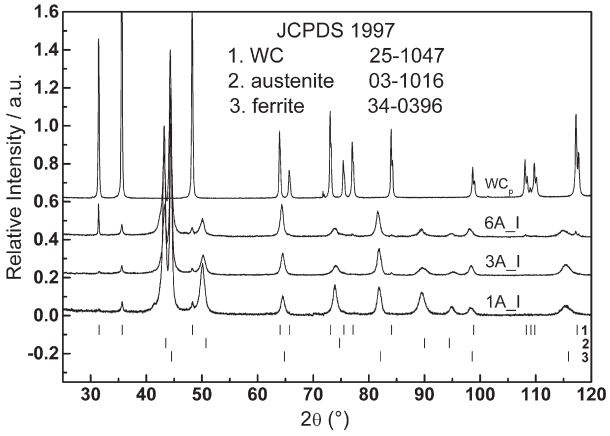

Fig. 8. Comparison of XRD spectra measured after LMI for all three duplex steels from Table 1. For comparison the spectrum measured on pure WC particles is also shown.

Fig. 8 demonstrates the XRD diffraction spectra taken from the surfaces of all three duplex steels treated by LMI process. No other phases than ferrite, austenite and WC were detected. However, from the higher relative intensity of austenite peaks in comparison with the remelting material (Fig. 4) one may expect that the matrix contains more austenite than just remelted laser track. The presence of the austenitic phase near injected WC particles was confirmed later by the phase contrast observation in OIM (see Fig. 10b). More detailed microstructural analysis confirms the presence of other phases, especially in the vicinity of WC particles, but probably due to their small quantities they have not been identified by XRD.

OIM mapping [22] was also used to study the details of the microstructure formed during laser melt injection. Fig. 9 demonstrates OIM mapping of two close particles injected in duplex steel matrix. It is seen that each WC particle contains many individual grains with an average size of about 10–20μm.

Fig. 10 summarizes oriented image microscopy analysis made in the vicinity of WC particles injected into duplex steel matrix. The image quality map shown in Fig. 10a demonstrates that a relatively narrow dark area (~ 10μm) around each particle exists. Inside this area the quality of the back-scattered diffraction patterns is too low making indexing impossible. The phase contrast mapping (Fig. 10b) clearly identifies the WC phase (yellow) inside the particles, the austenite (green) in distances between 10 and 50μm from particles gradually decreases with this distance and finally the ferrite (red) which gradually increases its presents in the same area.

Basically two different types of microstructures inside the reaction zone between WC particles and steel surrounding were observed. Fig. 11 shows one of them, when W_2C phase islands are detected nearby WC particles. More far from the WC particle the individual cells with ferritic cores and austenitic shells around are present, as Fig. 10 demonstrates. The W_2C islands provide sometimes relatively very good EBSD pattern, which can be indexed and crystallographic orientation of this phase may be compared with crystallographic orientation of grains in WC particle. Fig. 11 also shows graphically the crystallographic orientation of two neighborhood grains in WC

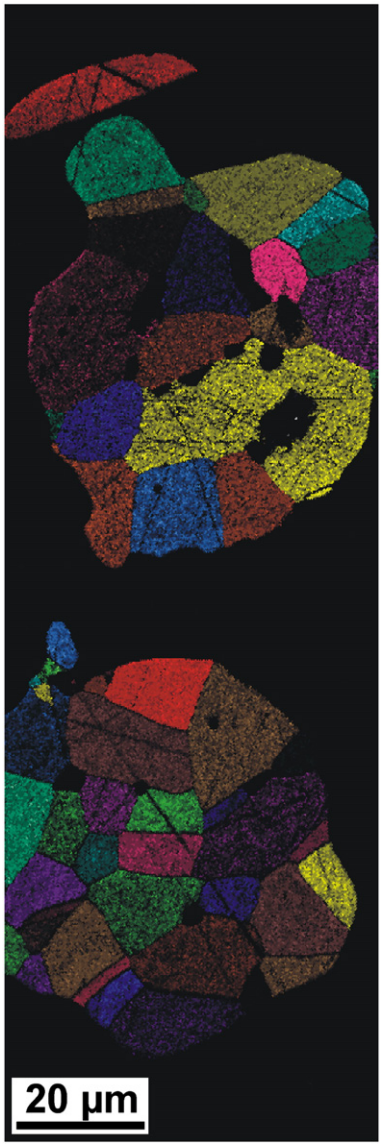

Fig. 9. OIM analysis of injected WC particles. Different grains detected by OIM in two close WC particles injected in duplex steel. The indexed Kikuchi pattern of WC phase showing hexagonal structure with $P\bar{6}m2$ symmetry group and lattice parameters of $a=2.91$ and $c=2.84$ Å.

particle together with crystallographic orientations of W_2C islands in their vicinity. It was observed, that between these two phases the clear orientation relationship exists:

$$\left[1\,\bar{2}\,10\right]_{W_2C}//\left[1\,\bar{2}\,10\right]_{WC},(0001)_{W_2C}//(0001)_{WC} \quad (1)$$

The second type of microstructure observed in the vicinity of WC particles is shown in Fig. 12. The reaction zone does not contain W_2C phase islands near the WC particle, but three distinguishable zones may be defined, similar as in observations made in [23] where functionally graded WC coatings prepared by laser cladding technique are reported. Each of these zones has its own characteristic microstructure and iron/tungsten composition, detected by EDS and summarized in Table 2.

4. Discussion

Several research papers in literature have concentrated on the correlation between the chemical composition of stainless and duplex steels and their solidification mode. Particularly the ratio of Cr_{eq} and Ni_{eq} and solidification rate are reported as parameters which control the solidification mode [24,25]. In this work we confirmed by microstructural observations that during casting and also during fast solidification after laser remelting the ferrite is the phase which solidifies first. Taking into account that all duplex steels used in our study show $Cr_{eq}/Ni_{eq} > 2.0$, this observation is in agreement with the concept of a microstructural map, as a function of composition and solidification growth rate over a wide range of solidification conditions proposed for austenitic stainless steels by Lippold [26]. The agreement with other observations [27–29] should be also noticed.

The OIM technique based on indexing of electron back-scattered patterns has shown to be a powerful instrument for microstructural study of MMC coatings created by LMI technique. Interesting observations concerning orientation relationship between ferritic and austenitic grains formed during casting of duplex steel have been also performed, and details will be published elsewhere [20].

Hardening observed after simple laser surface remelting is caused mainly by ferritization, when practically the whole remelted volume is transformed to ferrite. However, the influence of laser beam scanning speed, which mainly determines the cooling rate, is also pronounced, when laser tracks remelted with higher laser beam scanning speeds results in coatings with higher hardness (see Fig. 5). On the other hand, in the case of laser melt injection, an increase of the hardness of the matrix is caused by dissolution of W and C into steel matrix and by a formation of hard phases near particle/matrix interfaces. This hard matrix may be an additional factor together with the presence of ceramic particles, which may increase the performance of this coating in wear applications. Experimental observations of performance of these coatings in dry sliding wear tests in comparison with non-treated casting duplex steel surfaces are in progress.

Recently, WC reinforced surface metal matrix composite produced by plasma melt injection into low carbon steel was reported [30]. However, due to the higher thermal impact into the substrate during plasma forming by transferred plasma arc, a substantial larger part of WC particles is dissolved into the melt matrix, forming microstructures in which only a small part of injected particles remains untouched. The higher cooling rate, which is characteristic for laser surface processing techniques, leads to the formation of microstructure when the injected particles retain their size if the direct contact between the laser beam and the particles stream is minimized.

As the laser power was kept constant during the LMI process and the substrate samples were quite small, one may observe in Fig. 6b a progressive increase of remelted depth of laser track from left to the right due to a gradual increase of the substrate temperature. Because the temperature of the substrate and the melt pool was not monitored during the laser melt injection process we decided do not change the laser power from the beginning to the end of the process with a risk that the size of the

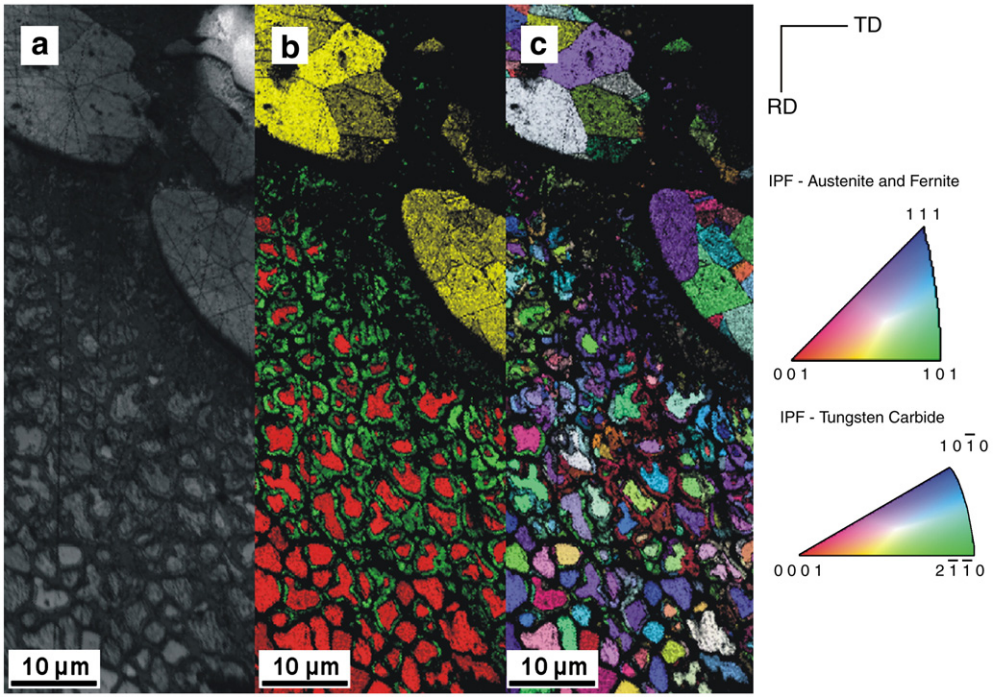

Fig. 10. OIM analysis of reaction zone between WC particles and remelted duplex steel matrix. a) Image quality picture; b) Phase contrast mapping; c) Inverse pole figures for orientation of austenite, ferrite and WC grains.

laser track will gradually increase. However, it seems to us that the observed increase in depth is not so substantial that a dramatic influence on microstructure and properties has to be expected. To solve this problem in the future a gradual reduce of laser power during processing may be arranged or a design of powerful cooling on the bottom side of the disk substrate has to be realized.

However, one may conclude from Fig. 6b that an optimal overlapping for this combination of processing parameters has to be larger, to achieve a reasonable thickness of MMC coating also in the overlapping areas. Therefore, an optimal displacement for subsequent laser track has not to be estimated from the width of simple remelting laser track (as it was in case shown in Fig. 6b), but from the width of laser track formed during laser melt injection, because the injected particles partially shield laser beam which results in a reduction of energy used for substrate melting and subsequently in a reduction of laser track width.

Two different types of reaction zone formed near the interface between steel matrix and WC particle (see Figs. 11 and 12) may be explained as interfaces created in a reaction between the steel melt and "cold" or "hot" WC particle surface, respectively. It is characteristic for laser melt injection set-up, that the stream of powder particles is located just below the traveling laser beam aiming at minimizing the interaction between laser beam and injected particles [5]. Nevertheless, a part of the powder stream

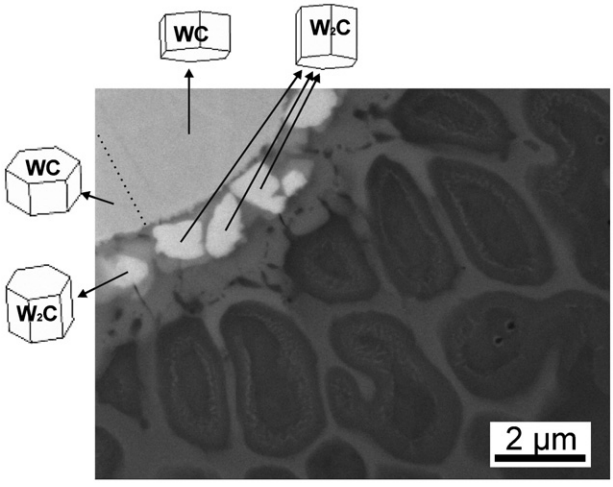

Fig. 11. Orientation relationship analysis between grains in WC particle and W_2C phase detected in very close vicinity of "cold" WC particles. A graphical representation of crystallographic orientation relationship detected between grains in WC particles and small islands of W_2C phase presented nearby and indexed as: Trig. ($P\bar{3}m1$) a=2.98 and c=4.71 Å.

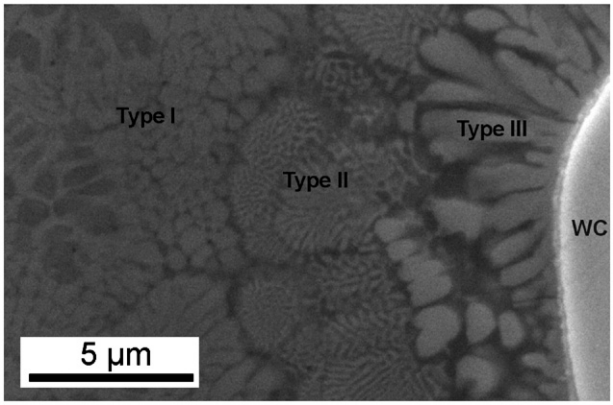

Fig. 12. Three distinct zones near "hot" WC particle observed by SEM.

Table 2
Iron and tungsten content (in wt%) detected by EDS inside WC particle and three zones defined in Fig. 12.

	Fe wt.%	W wt.%
WC particle	0.8	94.0
Type I	47.5	16.0
Type II	44.7	27.4
Type III	28.6	47.0

intersects with the laser beam and these particles reach the melt pool as "hot" particles. Their surface may be overheated to very high temperatures close to the melting point of WC (2870°C) or are even melted. This reduces the final particle size and creates the eutectic phases localized close to particle that are rich in W and C. These particles can be generally recognized in the coating as particles with smaller size. For these particles the characteristic reaction zone shown in Fig. 12 is formed. On the other side the "cold" particles create a reaction zone mainly via dissolution of C and W into surrounding melt, as a formation of W_2C islands with strong OR to original WC grains from particle indicates. However, the fact that a reaction zone between matrix and injected WC particles is formed may result in a strong bonding and a good performance in wear applications, as it was observed in the case of Al and Ti alloys [31,32].

5. Conclusions

The laser surface remelting of duplex steel results in epitaxial/columnar grains grown in the melt pool and in a small increase of microhardness due to ferritization and microstructure formed by high cooling rates. The large processing window offers coatings free of cracks and pores.

The laser melt injection of WC particles into duplex steels results in a metal matrix composite coating with a substantial increase of the matrix hardness due to C and W presence in the reaction zone. Two types of reaction zone between WC particles and steel matrix were identified. Reaction zone with eutectic phases rich in W and C; and reaction zone characterized by W_2C islands with the strong orientation relationship to the original grains of WC particle.

The processing window of laser melt injection process is limited mainly due to cracking when a higher amount of WC particles is injected.

Acknowledgment

The work reported was carried at University of Groningen during a leave of absence from University of Campinas by A.M. Do Nascimento. The authors acknowledge the financial support provided by The Scientific Research Foundation of the State of São Paulo, Brazil, FAEPEX-Unicamp, CNPq (The Brazilian Research Council), Capes and The Netherlands Institute for Metals Research. Dr. Marcelo Martins from Sulzer Brazil S/A — Fundinox Division is acknowledged for providing with duplex steel experimental materials.

References

[1] A.B. Kloosterman, B.J. Kooi, J.Th.M. De Hosson, Acta Mater. 46 (1998) 6205.
[2] J.A. Vreeling, V. Ocelík, Y.T. Pei, J.Th.M. De Hosson, in: C.A. Brebbia, J.M. Kenny (Eds.), In Surface treatment IV, Computer Methods and Experimental Measurements, WitPress, Southampton, Boston, 1999, pp. 269–278.
[3] J.A. Vreeling, V. Ocelík, Y.T. Pei, D.T.L. van Agterveld, J.Th.M. De Hosson, Acta Mater. 48 (2000) 4225.
[4] J.A. Vreeling, V. Ocelík, J.Th.M. De Hosson, Acta Mater. 50 (2002) 4913.
[5] Y.T. Pei, V. Ocelík, J.Th.M. De Hosson, Acta Mater. 50 (2002) 2035.
[6] P. Krull, H. Pries, H. Wohlfahrt, J. Tosch, Weld. Res. Abroad 44 (1998) 2.
[7] J. Olsson, B. Leffler, C. Jorgensen, Proceedings of the 9th International Symposium on Corrosion in the Pulp and Paper Industry, Montreal, Canada, 1996, p. 161.
[8] K. Tersmeden, Proc. Saf. Prog. 16 (1997) 110.
[9] R.N. Gunn, Duplex Stainless Steels—Microstructure, Properties and Applications, Abington Publishing, Cambridge, 1997, p. 6.
[10] W. Cerri, R. Martinella, G.P. Mor, P. Bianchi, D.D. Angelo, Surf. Coat. Technol. 49 (1991) 40.
[11] B.D. Zhu, X.Y. Zeng, Z.Y. Tao, S.G. Yang, K. Cui, Wear 170 (1993) 161.
[12] Z.D. Chen, L.C. Lim, M. Qian, J. Mater. Process. Technol. 62 (1996) 321.
[13] M. Cadenas, R. Vijande, H.J. Montes, J.M. Sierra, Wear 212 (1997) 244.
[14] A. Hidouci, J.M. Pelletier, F. Ducoin, D. Dezert, R. El Guerjouma, Surf. Coat. Technol. 123 (2000) 17.
[15] M. Brandt, S.W. Huang, M. Samandi, J. Laser Appl. 15 (2003) 31.
[16] K. van Acker, D. Vanhoyweghen, R. Persoons, J. Vangrunderbeek, Wear 258 (2005) 194.
[17] C. Navas, R. Colaco, J. de Damborenea, R. Vilar, Surf. Coat. Technol. 200 (2006) 6854.
[18] D.J. Kotecki, T.A. Siewert, Weld. J. 71 (1992) S171.
[19] J. Charles, Super Duplex Stainless Steel: Structure and Properties, 2nd. Duplex Stainless Steels, 1991.
[20] A.M. Do Nascimento, V. Ocelík, M.C.F. Ierardi, J.Th.M. De Hosson, Crystallographic orientation relationships between ferrite and austenite in casting duplex steels, to be published.
[21] U.O.B. de Oliveira, *Laser treatment of alloys: processing, microstructure and structural properties*, PhD Thesis, 128 pp. 2007. Groningen, Rijksuniversiteit Groningen.
[22] A.J. Schwartz, M. Kumar, B.L. Adams (Eds.), Electron Backscatter Diffraction in Materials Science, Kluwer, New York, 2000, 339pp.
[23] M. Riabkina-Fishman, E. Rabkin, P. Levin, N. Frage, M.P. Dariel, A. Weisheit, R. Galun, B.L. Mordike, Mater. Sci. Eng. A302 (2001) 106.
[24] N. Suutala, Metall Trans., A 14A (1983) 191.
[25] J.M. Vitek, S.A. David, C.R. Hinman, Weld. J. 82 (2003) S10.
[26] J.C. Lippold, Weld. J. 73 (1994) S129.
[27] T. Takalo, N. Suutala, T. Moisio, Mettal. Trans. A 10A (1979) 1173.
[28] J.A. Brooks, J.C. Williams, A.W. Thompson, Mettal. Trans. A 14A (1983) 1271.
[29] K. Rajasekhar, C.S. Harendranath, R. Raman, S.D. Kulkarni, Mater. Charact. 38 (1997) 53.
[30] M.H. Zhao, A.G. Liu, M.H. Guo, D.J. Liu, Z.J. Wang, C.B. Wang, Surf. Coat. Technol. 201 (2006) 1655.
[31] V. Ocelík, D. Matthews, J.Th.M. De Hosson, Surf. Coat. Technol. 197 (2005) 303.
[32] R. Anandkumar, A. Almeida, R. Colaço, R. Vilar, V. Ocelik, J. Th. M. De Hosson, Surf. Coat. Technol. 201 (2007) 9497.
[33] J.O. Nilsson, Mater. Sci. Technol. 8 (1992) 685.